


ORIGINAL ARTICLE

Monte Carlo Code Calculation for the Characterization of 10nm Nano-Layers Coated 50nm ⁹⁰Y Radionuclide Nanospheres Radiation in the Liver Radionuclide Therapy

Farshad Seyednejad ^{1,2}, Hosein Ghiasi ^{1*} 

¹ Medical Radiation Research Team, Tabriz University of Medical Sciences, Tabriz, Iran

² Department of Radio-Oncology, Medical School, Tabriz University of Medical Sciences, Tabriz, Iran

*Corresponding Author: Hosein Ghiasi
Email: hoseinghiasi62@gmail.com

Received: 26 June 2021 / Accepted: 12 October 2021

Abstract

Purpose: Cancer radionuclide therapy is an effective, beneficial, and crucial method of cancer treatment that uses unsealed radioactivated radionuclides sources that are attached to a targeting vector to deliver therapeutic radiation doses from the ionizing radiation source to specific disease sites either for curative intent or for disease control and palliation for the patient pain decreasing. For this aim, Monte Carlo N-Particle 5 (MCNP5) MC computational code was employed for simulations and calculations as well as radiation transport.

Materials and Methods: 50nm ⁹⁰Y radionuclide nanosphere was modelled coated by a 10nm coating layer with some non-toxic high and low Z materials. Physical interactions, such as β -ray and the simulated coating materials were studied and radiological parameters were scored by the used MC code. Attenuation of β -ray, and production of the bremsstrahlung X-ray photons and other phenomena were simulated by the code and analyzed. MC code estimated the effect of the simulated coating materials, such as Gold, Platinum, Gadolinium, Silver, and Epoxy-Resin on the radiation characteristics around the modelled nano-radionuclide per 2nm from the radiation source surface to 1 μ m distance. Produced bremsstrahlung X-ray by the source coating material and tissue atoms, emitted β -particle number, flux over the surfaces (per 2nm), radiation fluence of photon and β - ray, deposited energy per gr of the cell medium, and average dose to the cells around the 500nm and 1 μ m distance from the radionuclide source surface also was derived.

Results: Our results showed that coating the radionuclide with the materials especially high Z (Gold and Platinum) materials may produce a dual emitter radiation source, X-ray photon and β - ray and is capable of killing the cancer cells more than the source with not-coated source.

Conclusion: Our conclusion was that coating the β - ray emitter radionuclides, especially high-energy β - ray, enhances its therapeutical capability with X-ray and β - ray emission. The studied coated sources in our study were performed as a dual radiation source; produced X-ray and β -ray, which increases the therapeutic efficiency of the source.

Keywords: Nanospheres; ⁹⁰Y Nanospheres; Monte Carlo N-Particle; Monte Carlo Simulation; Radionuclide Therapy.

1. Introduction

Cancer radionuclide therapy is a radiation therapy modality that unsealed radioactivated radioisotope nuclides are employed to deliver therapeutic radiation doses from the ionizing radiation sources to the malignant sites either for curative intent or for cancer control and pain palliation for the patient pain decreasing. Some radionuclides have attracted radiotherapists and oncologists for the patient's cancer treatment and palliation and, are been used widely worldwide [1-30]. From the β -ray emitter radionuclides which were used for the cancer radionuclide therapy, the ^{14}C , ^{199}Au , ^{177}Lu , ^{131}I , ^{90}Sr , ^{153}Sm , ^{186}Re , ^{32}P , ^{90}Y , ^{38}Cl , and ^{88}Rb can be mentioned. ^{90}Y radionuclide is a pure β -ray emitter radionuclide that has a physical half-life of ≈ 2.7 days or 64.8 hrs. The mean and maximum energies (E_{mean} and E_{max}) of the pure β -ray emitter ^{90}Y radionuclide were reported as 0.933 MeV and 2.280 MeV, respectively. The average and maximum range of the emitted β - particles from ^{90}Y radionuclides are 4 and 11.3 mm in water, respectively [31;32]. As soft tissue composition and dosimetric characteristics are similar to water, the particle ranges in the soft tissue may be very closer to that in the water. The dose rate of the simulated ^{90}Y radionuclide source in the water reported as being calculated from the below-given equation, which depends on the radionuclide decay constant and its decay time; where (\dot{D}_0) is the initial dose rate of the studied source, λ stands for the source decay constant, m shows the target material mass, T is the total irradiation time and, $A(t)$ is the radionuclide radioactivation as a function of time that represents the number of β -particles (i.e. number of decays) emitted per second from the source with energies randomly selected from the ^{90}Y β -ray spectrum (Equation 1).

$$D(t) = \frac{A(t)}{m} = \dot{D}_0 e^{-\lambda t} \quad (1)$$

Additionally, total doses from the radionuclide were calculated according to the below relation for varying the ^{90}Y radionuclide concentrations using the full β -energy spectrum of ^{90}Y radionuclide (Equation 2):

$$D = \int_0^T \dot{D}(t) dt = \dot{D}_0 \int_0^T e^{-\lambda t} dt = \frac{\dot{D}_0}{\lambda} (1 - e^{-\lambda T}) \quad (2)$$

Physically, absorbed doses from the ^{90}Y radionuclide were calculated to be 1–10 Gy for Low Dose Rate irradiation (LDR) and close to 6–62 Gy for High Dose Rate irradiation (HDR), respectively [33]. Nowadays, radionuclide cancer radiotherapy is used widely as a

standard approach to cancer radiation therapy and, its therapeutic outcome has been reported as good in some cancer treatments such as liver, lung, and brain cancers [1-8]. The researchers in the radiotherapy-oncology of medicine brunch and cancer radiation therapy have been interested in the optimized use of systemic targeted radionuclide cancer therapy methods. Mahnken investigated pure β -emitter ^{90}Y radionuclide and reported promising results for the liver metastasis treatment and removal [34]. In Lobbe *et al.* [8] study, an explanation of the reported normalization scheme applied to the radionuclides calibration factors has been provided. They provided data on the effect of low observed current output due to depleted gas in the chamber is examined using the simulated derived data, comparisons of the derived normalized calibration factors to the measurement data for a variety of radionuclides, and finally, almost all of the secondary standards produced data are of radionuclides for distribution to the nuclear medicine community [33; 35]. The application of the ^{90}Y for the liver radionuclide radiotherapy has been carried out by injecting the radionuclide from the liver port vein and entering it to the liver blood circulatory system and distribution in the liver organ tissue. ^{90}Y nanospheres offer an advantage over microspheres that avoids thrombosis and distribute close to uniform without significant thrombosis which blocks capillaries and does not allow the radionuclide source to a uniform distribution. Although microspheres of the ^{90}Y were researched and applied in the clinic, using nanospheres of the ^{90}Y sources increases the advantages more than micro-scale ^{90}Y [36-38]. Maarten *et al.* [39] reviewed the Intra-Arterial radioembolization of breast cancer liver metastases, and their main conclusion was that the results from the study showed that ^{90}Y -Radioimbolzation is an effective treatment method for breast cancer and liver metastases removal. Comparative studies, mainly combining ^{90}Y radionuclide Radioinmolization with systemic radiation therapy are supported and encouraged in the main conclusion of Maarten *et al.*'s work [39]. ^{90}Y , which dosimetrically is a pure β -emitter with an energy spectrum from the 0-2.28 MeV, and a β -particle emitter source have E_{max} and E_{mean} of 2.28 MeV and 0.651 MeV and specific activity of 400 MBq/mg [40]. The source extraction reported in (^{89}Y , ^{90}Y) nuclear reaction and is activated by neutron activation that reaches its stable state by decaying to ^{89}Zr . Although the radionuclide is a pure β -source, in the current study, the nano-scale of the sources were coated by materials in nm-scale and some cases such as high Z materials, including gold and platinum, bremsstrahlung X-ray

photons production, and β -particles attenuation were simulated by the MCNP5 computational code. The authors aimed to analyze radiation around some high, medium, and low Z materials coated-⁹⁰Y radionuclide nanosphere by the materials and the characterization of the source radiation characteristics around 500 nm and 1 μ m distances from the radiation source.

2. Materials and Methods

Monte Carlo all-purpose N-Particle transport code (MCNP) version 5/1.60 was used to simulate and calculate in the current study. The complicated problem physics and complex geometry simulations of the problem were conducted by the MC code capabilities. The calculation of the dosimetric characteristics was carried out employing the rich physics databases and libraries, including the physical cross-sections of the materials and radiation physical interactions phenomena. The used MC code is capable of modelling three-dimensional complex geometries and physics in three-dimensional space and solving the problems based on a numerical calculation approach. In our previous studies, the MC simulation method was employed for nanoparticle radiation dose modification and the MC estimation was validated for physical and radiation properties characterization in the radiation field [40].

A 50 nm spherical source cell was modelled as ⁹⁰Y radionuclide nanosphere coated by a 10 nm nanolayer made of Platinum, Gold, Silver, and Epoxy Resin materials separately in the separate programmed input files. The radiation field of the ⁹⁰Y radionuclide nanosphere, around the radionuclide, was characterized coated by the source surface nanolayers in 10 nm thick per 2 nm and also and for bare source for comparison. The coated nano-scale simulated 10 nm materials were chosen for the high, medium, and low Z materials considered in the modelling of the problem for the effect of the nano-source coating materials on the ⁹⁰Y radionuclide nanosphere pure β -particle emitter radiation investigation. The employed MCNP5 code modelled 50 nm nano-source with the coating of the 10 nm nanolayer performance as a dual-energy source due to bremsstrahlung X-ray photon radiation and pure β -particle emitters scored by the use of the MC computational MCNP5/1.60 code and the code derived results were discussed. Physical interaction data derived from the β -particles and around by the modelled 10 nm coating nanolayer was the origin of the bremsstrahlung X-ray photons production around the MC simulated ⁹⁰Y

radionuclide nanosphere in the patient soft tissue. According to radiation physics, Auger electrons can be found in the radiation field around the radionuclide emitted radiation with the orbital elections and included in the code calculation for the radiation field around the nano-scale simulated pure β -particle emitter ⁹⁰Y. Stopping the β -particles in the soft tissue and conversion of its particles radiation energy to the X-ray photons that consequently attenuates the emitted β -particle in the tissue can be considered as an X-ray photon production origin and coating the source with a 10 nm high, medium, and low Z source and makes it a dual radiation types source; X-ray photons and the pure β -particle emitter source at some nm around the radionuclide nanosphere simulated source. MC employed MCNP5/1.60 code calculation for the radiation characterization was precisely conducted by code calculation per simulated 2 nm surfaces from the source surface and the cells between the modelled surfaces to 1 μ m from the radionuclide source. The scored physical and dosimetric parameters of the radiation source were precisely estimated running the programmed input files calling for the rich cross-sections physics database of the MC used code. The used MCNP code derived dosimetric characteristics of the radiation field estimated with statistic error lower than 0.01.

The application of the MC code tallies and the simulated surfaces with distances of 2 nm from each surface for radiation dosimetric characteristics allowed us to store radiation dosimetric parameters from the radionuclide source surface. MC MCNP5/1.60 code tallies were defined in a separately programmed input files data card that includes problems physics aspects and materials characteristics, as well as required dosimetric characteristics scoring the radiation field dosimetric parameters; F1 tally that scores the number of photons and β -particles; F2 tally that calculates particle and photon flux averaged over a surface in $1/\text{cm}^2$; the employed F4 tally of the code estimates tracks length of particle and photon flux in $1/\text{cm}^2$; *F8 is an MCNP code tally which calculates deposited energy from the ionizing radiation in MeV to the MC code defined cell medium and geometry. Employing the described tallies, photon, and β -particle radiation was characterized from a ⁹⁰Y radionuclide nanosphere radiation around some nm modeled the simulated radionuclide and absorbed dose from the photon and β -particle radiation in defined cells around the radionuclide source of the ionizing radiation. Annals of the International Commission on Radiological Protection (ICRP) that was released recently in 2021 on the "Use of Dose Quantities in Radiological

Protection”, reported radiation absorbed dose as the essential quantity for the risk estimations and dosimetric calculations that is the improved version of the ICRP 103 annual report. Radiation absorbed dose around the ^{90}Y radionuclide nanosphere source was calculated considering the radiation source deposited energy into the cell mass and geometry of the cells. The average energy deposited from the radiation source into the cell material mass has been defined as given below Equation [41;42]:

$$D = \frac{d\bar{E}}{dm} \quad (3)$$

Where D stands for the absorbed dose in Gy from the radiation source, $d\bar{E}$ is the average energy deposited into the mass in Kg in the MC code-defined cells between the modeled surfaces with 2 nm around the 50 nm source with the 10 nm coating layer.

3. Results and Discussion

MCNP5/1.60 of the MC code simulation was used for the ^{90}Y radionuclide nanosphere emission characterization coated by different materials nano-layers as well as X-ray radiation estimation around the modeled 50 nm nano-scale source and 10 nm nano-layer different material. 10 nm coated source from different materials around 50 nm produced a bremsstrahlung X-ray photon radiation 17% of the β -particle radiation emitter for the gold as the heist in Z on average over the 50 nm around the source. In Tables 1 and 2, the code-derived radiation dosimetric characteristics were presented. Bremsstrahlung X-ray produced in the resin and gold nano-shell interaction with high energy β -particle radiation was shown as effective radiation in the cells absorbed dose or local dose absorption. The photon beam produced a thorough bremsstrahlung phenomenon, associated with an energy spectrum with the endpoint of 2.28 MeV. Such an energetic photon contributed to the cell's absorbed dose equivalent and increases local dose enhancement which kills cells and damages malignant cells. X-ray produced in the resin and gold nano-shell interaction with high energetic β -particle radiation was shown as effective radiation in the cells absorbed dose. The photon beam produced a thorough bremsstrahlung phenomenon, associated with an energy spectrum with the endpoint of 2.28 MeV. Such energetic photons contributed to the cell's absorbed dose equivalent and increases local dose enhancement which kills cells and damages malignant cells. Dose increase due to bremsstrahlung X-ray for resin and gold nano-shell

embedded nano-radionuclide therapy observed for Platinum, Gold, Silver, and Epoxy Resin up to 31.08%, 41.00%, 29.78, and 29.09%, respectively in close vicinity of the ^{90}Y radionuclide. Our calculation showed minimum and the maximum portion of bremsstrahlung X-ray in total dose equivalent for Platinum, Gold, Silver, and Epoxy Resin 23.71%, 29.07%, 22.94%, and 22.53%, respectively. Because target materials' atomic number is different, the energy and mean energy of the produced bremsstrahlung X-ray was different, and for example in the case of Gold which is used for medical accelerators target, we derived the average energy of X-ray as 0.676 MeV and it may be low for other materials due to their lower atomic number comparing to Gold.

For the nano radionuclide source coated by different nano-materials, the number of bremsstrahlung X-ray photons per source β -particles emission was derived for 20 nm gold-coated and silver-coated sources with 1.12 and 9.83×10^{-1} times of a source without any coating material as maximum configurations and minimum configuration from the source surface to 1 μm from the source surface in average. The number of photons, photon flux averaged over a surface in $1/\text{cm}^2$, estimated track length of photon flux in $1/\text{cm}^2$, and derived energy deposition from the X-ray radiation in MeV to a defined medium were tabulated in Tables 1(A) and 1(B). Table 1(B) shows the MC code calculated effect on the coated materials in the values of the parameters. The average tally was estimated parameters from the source surface to 1 μm and 500nm from the source surface.

Additionally, calculated parameters for β -particle radiation was also tabulated in Tables 2(A) and 2(B) where the effect of the coating material was shown in Table 2(B).

Derived data by the MC code calculation revealed the effect of 10nm coating material with different Z, that in the calculated data, Gold's effect in X-ray production and increasing in photons both in 500 nm and 1 μm from the source is more than the other materials. On the other hand, Platinum, with an atomic number close to the Gold effect was seen very near to the gold. Another reason for the atomic number's high effect is the lowest effect of the Epoxy Resin which in most cases data in presence of it was the same as the soft tissue. For X-ray photon number, flux over a surface, fluence, and deposited energy, according to Tables 1(A) and 1(B), the maximum increase in data observed for the 10 nm gold-coated source and the minimum effect was observed for 10 nm Epoxy-Resin coated ^{90}Y

Table 1A. MCNP5 MC code tallies estimated bremsstrahlung X-ray dosimetric values per initial ^{90}Y radionuclide nanosphere β -emission 500 nm and 1 μm around the radionuclide

Estimate Value	The average tally estimated value from the source surface to 1 μm				The average tally estimated value from the source surface to 500 nm				
	MCNP5 TALLY	F1 tally	F2 tally	F4 tally	*F8 tally	F1 tally	F2 tally	F4 tally	*F8 tally
Platinum Coated-Source		6.86×10^{-6}	9.46×10^3	9.39×10^3	1.44×10^{-5}	7.22×10^{-6}	9.95×10^3	9.88×10^3	1.52×10^{-5}
Gold-Coated Source		6.95×10^{-6}	9.46×10^3	9.39×10^3	1.46×10^{-5}	7.31×10^{-6}	9.95×10^3	9.88×10^3	1.54×10^{-5}
Silver-Coated Source		6.11×10^{-6}	9.62×10^3	9.00×10^3	1.14×10^{-5}	6.43×10^{-6}	1.01×10^4	9.47×10^3	1.20×10^{-5}
Gadolinium-Coated Source		6.23×10^{-6}	9.69×10^3	9.01×10^3	1.19×10^{-5}	6.55×10^{-6}	1.02×10^4	9.48×10^3	1.26×10^{-5}
Epoxy-Resin-Coated Spouse		6.23×10^{-6}	9.25×10^3	8.89×10^3	1.01×10^{-5}	6.55×10^{-6}	9.72×10^3	9.35×10^3	1.06×10^{-5}
Bare Source		6.22×10^{-6}	9.25×10^3	8.89×10^3	1.00×10^{-5}	6.54×10^{-6}	9.72×10^3	9.35×10^3	1.05×10^{-5}

Table 1B. MCNP5 MC code tallies estimated bremsstrahlung X-ray dosimetric values per initial ^{90}Y radionuclide nanosphere β -emission 500 nm around the radionuclide ratio to the source without any coated layer

Estimate Value	The average tally estimated value				Estimated dosimetric value from the source surface to 500nm				
	MCNP5 TALLY	F1 tally	F2 tally	F4 tally	*F8 tally	F1 tally	F2 tally	F4 tally	*F8 tally
Platinum Coated-Source		1.10	1.02	1.06	1.44	1.10	1.02	1.06	1.45
Gold-Coated Source		1.12	1.02	1.06	1.47	1.12	1.52	1.06	1.47
Silver-Coated Source		9.83×10^{-1}	1.04	1.04	1.14	9.81×10^{-1}	1.54	1.01	1.14
Gadolinium-Coated Source		1.00	1.04	1.01	1.19	1.00	1.04	1.01	1.20
Epoxy-Resin-Coated Spouse		1.10	1.00	1.01	1.20	1.00	1.06	1.01	1.20
Bare Source		1.00	1.00	1.00	1.00	1.00	1.00	1.00	1.00

radionuclide nanosphere both in 500 nm and 1 μm from the source surface. For β -particle, also, gold coating performed as the maximum material for β -particle or electron increasing in the 500 nm and 1 μm from the source surface.

It may be attributed to the physical interactions of the photons and electrons in that more electrons are released in the photon and source emitted particles interactions. From the results of the current investigation, coating the ^{90}Y radionuclide nanosphere enhances both X-ray photon and secondary electron around the source and increases the source efficiency especially with high Z materials. Radiation absorbed dose (Gy) around 500 nm and 1 μm of 10 nm coated 50 nm spherical source was obtained associated with the coated-materials as following for

X-ray photons. Our MC simulation-derived data showed a significant effect of the high Z coating material on the X-ray production besides the β -ray emission and the bremsstrahlung effect. [Tables 1](#) and [2](#) compared X-ray and β -ray characteristics derived from the coated and non-coated ^{90}Y nano-radionuclide and derived data at 500 nm and 1 μm from the source surface which revealed the severe divergence in dosimetric parameters tallied by the code occurred at distances below 500 nm and after the distance, and a slightly observed difference was seen in both X-ray production and β -ray emission. There is no precise investigation on the physics of the nano-scale ^{90}Y nano-radionuclide conducted. We simulated surfaces and cells with 2 nm from the β -ray emitter nano-radioactive and it revealed detailed physical phenomena.

Table 2A. MCNP5 MC code tallies estimated β -particle dosimetric values per initial ^{90}Y radionuclide nanosphere β -emission 500 nm and 1 μm around the radionuclide

Estimate value	The average tally estimated value from the source surface to 1 μm				Estimated dosimetric value from the source surface to 500nm			
	MCNP TALLY	F1 tally	F2 tally	F4 tally	*F8 tally	F1 tally	F2 tally	F4 tally
Platinum Coated-Source	1.00	7.90×10^8	2.38×10^9	1.43×10^{-5}	1.05	8.31×10^8	2.51×10^9	1.51×10^{-5}
Gold-Coated Source	1.00	7.99×10^8	2.39×10^9	1.44×10^{-5}	1.05	8.40×10^8	2.51×10^9	1.52×10^{-5}
Silver-Coated Source	1.00	7.04×10^8	2.10×10^9	1.11×10^{-5}	1.05	7.40×10^8	2.21×10^9	1.17×10^{-5}
Gadolinium-Coated source	1.00	7.08×10^8	2.05×10^9	1.11×10^{-5}	1.05	7.44×10^8	2.16×10^9	1.17×10^{-5}
Epoxy-Resin-Coated Spouse	1.00	6.89×10^8	2.00×10^9	1.08×10^{-5}	1.05	7.25×10^8	2.10×10^9	1.14×10^{-5}
Bare Source	1.00	6.89×10^8	2.00×10^9	1.01×10^{-5}	1.05	7.25×10^8	2.10×10^9	1.06×10^{-5}

Table 2B. MCNP5 MC code tallies estimated β -particle dosimetric values per initial ^{90}Y radionuclide nanosphere β -emission 500 nm around the radionuclide ratio to the source without any coated layer

Estimate value	The average tally estimated value				Estimated dosimetric value from the source surface to 500nm				
	MCNP TALLY	F1 tally	F2 tally	F4 tally	*F8 tally	F1 tally	F2 tally	F4 tally	*F8 tally
Platinum Coated-source		1.00	1.15	1.19	1.42	1.00	1.15	1.20	1.42
Gold-Coated source		1.00	1.16	1.20	1.43	1.00	1.16	1.20	1.43
Silver-Coated source		1.00	1.02	1.05	1.09	1.00	1.02	1.05	1.10
Gadolinium-Coated source		1.00	1.03	1.03	1.09	1.00	1.0	1.03	1.10
Epoxy-resin-Coated spouse		1.00	1.00	1.00	1.06	1.00	1.00	1.00	1.08
Bare Source		1.00	1.00	1.00	1.00	1.00	1.00	1.00	1.00

4. Conclusion

The authors concluded that for high-energy β -ray emitter radionuclides, high Z and non-toxic materials coated radionuclides increase its efficiency by making it a dual radiation type emitter; X-ray and β -ray. In close vicinity of the cancer cells ability of the coated source cell killing increases with the high Z and non-toxic material such as Gold or platinum by the enhancement of efficiency of the β -ray radionuclides. Enhancement of dose and efficiency of β -ray emitter radionuclides by coating it with different non-toxic materials was the subject of our study. It was deduced that a) manufacturing the radionuclides in small (nm) scale for thrombosis avoiding and also uniform distribution of the nano-radionuclides

increases its efficiency. b) Coating the nano-scale β -ray emitter radionuclides, especially high energy β -ray and high Z materials coating, enhances its performance in the cancer radionuclide radiation therapy with both β -ray and X-ray irradiation of the cancer cells and our proposed method was that making effectiveness in the cancer treatment and maybe a trigger for new models of the radionuclides production. Future studies are strongly proposed by the authors.

Acknowledgments

The authors would like to thank Tabriz University of Medical Sciences for their supports.

References

- 1- Zgorelec, M. +áo+ítari-ç, D. Babi-ç, I. +áestak, M. Mesi-ç, A. Per-ìn, and B. Petrinc, "Effects of fertilization on radionuclide uptake by maize from an acidic soil in northwestern Croatia.", *Soil and Tillage Research*, vol. 212, p. 105030, (2021).
- 2- I. M. Costa, J. Cheng, K. M. Osytek, C. Imberti, and S. Y. A. Terry, "Methods and techniques for in vitro subcellular localization of radiopharmaceuticals and radionuclides.", *Nuclear Medicine and Biology*, vol. 98-99, pp. 18-29, (2021).
- 3- S. Rout, S. Yadav, and V. Pulhani, "Transfer of radionuclides from soil to selected tropical plants of Indian Subcontinent: A review.", *Journal of Environmental Radioactivity*, vol. 235-236, p. 106652, (2021).
- 4- M. Sahagia, E. L. Grigorescu, A. Luca, A. C. W+ntjen, C. Ivan, A. Antohe, and M. R. Ioan, "60 years of absolute standardization of radionuclides by coincidence counting methods in the Romanian metrology laboratory.", *Applied Radiation and Isotopes*, vol. 174, p. 109707, (2021).
- 5- B. Fi+vet, P. Bailly du Bois, and C. Voiseux, "Concentration factors and biological half-lives for the dynamic modeling of radionuclide transfers to marine biota in the English Channel.", *Science of The Total Environment*, vol. 791, p. 148193, (2021).
- 6- M. Peer-Firozjaei, M. A. Tajik-Mansoury, P. Geramifar, A. A. Parach, and S. Zarifi, "Implementation of dose point kernel (DPK) for dose optimization of ¹⁷⁷Lu/⁹⁰Y cocktail radionuclides in internal dosimetry.", *Applied Radiation and Isotopes*, vol. 173, p. 109673, (2021).
- 7- M. Radomirovi-ç, S. Stankovi-ç, M. Mandi-ç, M. Jovi-ç, L. J. Mandi-ç, S. Dragovi-ç, and A. Onjia, "Spatial distribution, radiological risk assessment and positive matrix factorization of gamma-emitting radionuclides in the sediment of the Boka Kotorska Bay.", *Marine Pollution Bulletin*, vol. 169, p. 112491, (2021).
- 8- J. Lubbe, B. R. S. Simpson, M. J. van Staden, and M. W. van Rooy, "The operation of an ionization chamber with depleted gas for radioactivity measurement: Calibration procedure and utilising normalized manufacturer's radionuclide factors.", *Applied Radiation and Isotopes*, vol. 170, p. 109633, (2021).
- 9- A. Dash, S. Chakraborty, M. R. A. Pillai, and F. F. Knapp, "Peptide Receptor Radionuclide Therapy: An Overview.", *Cancer Biotherapy and Radiopharmaceuticals*, vol. 30, no. 2, pp. 47-71, (2015).
- 10- A. Sundl+iv and K. Sj+green-Gleisner, "Peptide Receptor Radionuclide Therapy Gçô Prospects for Personalised Treatment.", *Clinical Oncology*, vol. 33, no. 2, pp. 92-97, (2021).
- 11- T. Mastren, A. Akin, R. Copping, M. Brugh, D. S. Wilbur, E. R. Birnbaum, F. M. Nortier, K. D. John, and M. E. Fassbender, "A reverse ²³⁰U/²²⁶Th radionuclide generator for targeted alpha therapy applications.", *Nuclear Medicine and Biology*, vol. 90-91, pp. 69-73, (2020).
- 12- S. Basu, R. V. Parghane, Kamaldeep, and S. Chakrabarty, "Peptide Receptor Radionuclide Therapy of Neuroendocrine Tumors.", *Seminars in Nuclear Medicine*, vol. 50, no. 5, pp. 447-464, (2020).
- 13- H. Ahmadzadehfar, M. Essler, K. Rahbar, and A. Afshar-Oromieh, "Radionuclide Therapy for Bone Metastases: Utility of Scintigraphy and PET Imaging for Treatment Planning.", *PET Clinics*, vol. 13, no. 4, pp. 491-503, (2018).
- 14- S. Severi, A. "Peptide receptor radionuclide therapy in patients with metastatic progressive pheochromocytoma and paraganglioma: long-term toxicity, efficacy and prognostic biomarker data of phase II clinical trials.", *ESMO Open*, vol. 6, no. 4, p. 100171, (2021).
- 15- N. Heynickx, K. Herrmann, K. Vermeulen, S. Baatout, and A. Aerts, "The salivary glands as a dose limiting organ of PSMA- targeted radionuclide therapy: A review of the lessons learnt so far.", *Nuclear Medicine and Biology*, vol. 98-99, pp. 30-39, (2021).
- 16- M. Lassmann, U. Eberlein, and J. Tran-Gia, "Multicentre Trials on Standardised Quantitative Imaging and Dosimetry for Radionuclide Therapies.", *Clinical Oncology*, vol. 33, no. 2, pp. 125-130, (2021).
- 17- W. Delbart, G. E. Ghanem, I. Karfis, P. Flamen, and Z. +. Wimana, "Investigating intrinsic radiosensitivity biomarkers to peptide receptor radionuclide therapy with [¹⁷⁷Lu]Lu-DOTATATE in a panel of cancer cell lines.", *Nuclear Medicine and Biology*, vol. 96-97, pp. 68-79, (2021).
- 18- T. Vaghaiwalla, B. Ruhle, K. Memeh, P. Angelos, E. Kaplan, C. Y. Liao, B. Polite, and X. Keutgen, "Response rates in metastatic neuroendocrine tumors receiving peptide receptor radionuclide therapy and implications for future treatment strategies.", *Surgery*, vol. 169, no. 1, pp. 162-167, (2021).
- 19- K. Fujieda, J. Kataoka, S. Mochizuki, L. Tagawa, S. Sato, R. Tanaka, K. Matsunaga, T. Kamiya, T. Watabe, H. Kato, E. Shimosegawa, and J. Hatazawa, "First demonstration of portable Compton camera to visualize ²²³Ra concentration for radionuclide therapy.", *Nuclear Instruments and Methods in Physics Research Section A: Accelerators, Spectrometers, Detectors and Associated Equipment*, vol. 958, p. 162802, (2020).
- 20- S. K. Suman, S. Subramanian, and A. Mukherjee, "Combination radionuclide therapy: A new paradigm.", *Nuclear Medicine and Biology*, vol. 98-99, pp. 40-58, (2021).
- 21- D. L. Bushnell and K. L. Bodeker, "Overview and Current Status of Peptide Receptor Radionuclide Therapy.", *Surgical Oncology Clinics of North America*, vol. 29, no. 2, pp. 317-326, (2020).
- 22- R. Ghahramani-Asl, F. Razghandi, and H. R. Sadoughi, "Dosimetric evaluation of several candidate radionuclides used in radionuclide therapy of bone metastases in an upper leg model.", *Radiation Physics and Chemistry*, vol. 176, p. 109082, (2020).
- 23- Y. Ohshima, H. Suzuki, H. Hanaoka, I. Sasaki, S. Watanabe, H. Haba, Y. Arano, Y. Tsushima, and N. S.

- Ishioka, "Preclinical evaluation of new α -radionuclide therapy targeting LAT1: 2-[^{211}At]astato- α -methyl-L-phenylalanine in tumor-bearing model.", *Nuclear Medicine and Biology*, vol. 90-91, pp. 15-22, (2020).
- 24- L. Bodei, H. Schöder, R. P. Baum, K. Herrmann, J. Strosberg, M. Caplin, K. Höberg, and I. M. Modlin, "Molecular profiling of neuroendocrine tumours to predict response and toxicity to peptide receptor radionuclide therapy.", *The Lancet Oncology*, vol. 21, no. 9, p. e431-e443, (2020).
- 25- S. J. Goldsmith, "Targeted Radionuclide Therapy: A Historical and Personal Review.", *Seminars in Nuclear Medicine*, vol. 50, no. 1, pp. 87-97, (2020).
- 26- P. E. Hartrampf, H. Hünscheid, O. Kertels, A. Schirbel, M. C. Kreissl, M. Flentje, R. A. Sweeney, A. K. Buck, B. Polat, and C. Lapa, "Long-term results of multimodal peptide receptor radionuclide therapy and fractionated external beam radiotherapy for treatment of advanced symptomatic meningioma.", *Clinical and Translational Radiation Oncology*, vol. 22, pp. 29-32, (2020).
- 27- J. Dhanani, D. A. Pattison, M. Burge, J. Williams, B. Riedel, R. J. Hicks, and M. C. Reade, "Octreotide for resuscitation of cardiac arrest due to carcinoid crisis precipitated by novel peptide receptor radionuclide therapy (PRRT): A case report.", *Journal of Critical Care*, vol. 60, pp. 319-322, (2020).
- 28- H. Zhou, Q. Zhang, Y. Cheng, L. Xiang, G. Shen, X. Wu, H. Cai, D. Li, H. Zhu, R. Zhang, L. Li, and Z. Cheng, " ^{64}Cu -labeled melanin nanoparticles for PET/CT and radionuclide therapy of tumor.", *Nanomedicine: Nanotechnology, Biology and Medicine*, vol. 29, p. 102248, (2020).
- 29- J. Garousi, E. von Witting, J. Borin, A. Vorobyeva, M. Altai, O. Vorontsova, M. W. Konijnenberg, M. Oroujeni, A. Orlova, V. Tolmachev, and S. Hober, "Radionuclide therapy using ABD-fused ADAPT scaffold protein: Proof of Principle.", *Biomaterials*, vol. 266, p. 120381, (2021).
- 30- A. Stankovi-ç, J. Mihailovi-ç, M. Mirkovi-ç, M. Radovi-ç, Z. Milanovi-ç, M. Ognjanovi-ç, D. Jankovi-ç, B. Anti-ç, M. Mijovi-ç, S. Vranje-ç, and P. Prijovi-ç, "Aminosilanized flower-structured superparamagnetic iron oxide nanoparticles coupled to ^{131}I -labeled CC49 antibody for combined radionuclide and hyperthermia therapy of cancer.", *International Journal of Pharmaceutics*, vol. 587, p. 119628, (2020).
- 31- S. Agostinelli, et al, "Geant4 simulation toolkit.", *Nuclear Instruments and Methods in Physics Research Section A: Accelerators, Spectrometers, Detectors and Associated Equipment*, vol. 506, no. 3, pp. 250-303, (2003).
- 32- S. Jan, G. et al "GATE: a simulation toolkit for PET and SPECT.", *Phys Med Biol*, vol. 49, no. 19, pp. 4543-4561, (2004).
- 33- INTERNATIONAL ATOMIC ENERGY AGENCY VIENNA, "THERAPEUTIC RADIONUCLIDE GENERATORS: $^{90}\text{Sr}/^{90}\text{Y}$ AND $^{188}\text{W}/^{188}\text{Re}$ GENERATORS.", *IAEA, Vienna*, 470, (2009).
- 34- Andreas H Mahnken, " ^{90}Y -glass microspheres for hepatic neoplasia.", *Future Oncol*, 11(9):1343-54, (2015).
- 35- Y. Caffari, P. Spring, C. Bailat, Y. Nedjadi, and F. Bochud, "Activity measurements of ^{18}F and ^{90}Y with commercial radionuclide calibrators for nuclear medicine in Switzerland.", *Applied Radiation and Isotopes*, vol. 68, no. 7, pp. 1388-1391, (2010).
- 36- H. Ahmadzadehfar, H. J. Biersack, and S. Ezziddin, "Radioembolization of Liver Tumors With Yttrium-90 Microspheres.", *Seminars in Nuclear Medicine*, vol. 40, no. 2, pp. 105-121, (2010).
- 37- V. Aleksandar, J. Drina, R. Magdalena, M. Zorana, M. Marija, S. Dragana, and V. Sanja, "Optimization of the radiolabelling method for improved in vitro and in vivo stability of ^{90}Y -albumin microspheres.", in *Applied Radiation and Isotopes*, 156:108984, (2020).
- 38- F. Biltekin, G. Ozyigit, M. Yeginer, M. Cengiz, D. Celik, F. Yildiz, F. Akyol, F. Zorlu, and M. Gurkaynak, "EP-1374 THE SECONDARY MALIGNANCY RISK ESTIMATION DUE TO THE NEUTRON CONTAMINATION IN 3D-CRT AND IMRT TREATMENT TECHNIQUES.", *Radiotherapy and Oncology*, vol. 103, p. S521-S522, (2012).
- 39- M. L. J. Smits, Nijsen, B. A. Zonnenberg, B. A. Seinstra, M. G. E. H. Lam, and M. A. A. J. van den Bosch, "Intra-arterial radioembolization of breast cancer liver metastases: A structured review.", *European Journal of Pharmacology*, vol. 709, no. 1, pp. 37-42, (2013).
- 40- Seyyed Mostafa Ghavami, Ghiasi Hosein, and Asghar Mesbahi, "MONTE CARLO MODELING OF THE YTTRIUM-90 NANOSPHERES APPLICATION IN THE LIVER RADIONUCLIDE THERAPY AND ORGANS DOSES CALCULATION.", *Nuclear Technology and Radiation Protection*, 31(1):89-96, (2016).
- 41- International Commission on Radiological Protection, "The 2007 Recommendations of the International Commission on Radiological Protection.", *ICRP*, 103, (2007).
- 42- International Commission on Radiological Protection, "Use of dose quantities in radiological protection," *Ann. ICRP*, 147, (2021).